iBMA-12.7 copolymer, at whose copolymer composition a minimum point appears, is smaller than those of the two copolymers neighboring with respect to the copolymer composition; this may lead to good miscibility with respect to molecular weight compared to the respective neighboring blends. Also, the tacticities of the nBMA·iBMA copolymers used here are scarcely dependent on the copolymer composition as shown in Table II.

Concerning the dependence of miscibility on the VAc content, miscibility should be less as the VAc content increases. However, Figures 4–6 do not explicitly show such a behavior. The phase separation temperature is determined by the molecular weight as well as the copolymer composition. The molecular weights of VC·VAc-87 and -81 are considerably small compared to that of VC·VAc-90 and also the molecular weight of VC·VAc-81 is larger than that of VC·VAc-87. Therefore, the wider miscibility region with respect to temperature for the VC·VAc-87 blends may be due to the comparably low molecular weight of VC·VAc-87.

For the present systems, if the respective VC·VAc copolymers are regarded as homopolymers as described above, the present systems are the blends of an A_{r_1} and $(C_xD_{1-x})_{r_2}$ type, where A, C, and D correspond to the VC·VAc, iBMA, and nBMA *monomers*, respectively. Then, the intermolecular χ can be written from eq 1 as

$$\chi = x\chi_{AC} + (1-x)\chi_{AD} - x(1-x)\chi_{CD} \quad (5)$$

As is clear from eq 5, the intermolecular χ can be positive in a certain range of the copolymer compositions even though all the segmental χ_{ij}'s are negative. Then, the following relation is satisfied at that temperature:[1,2,4,8]

$$|\chi_{CD}| > (|\chi_{AC}|^{1/2} + |\chi_{AD}|^{1/2})^2 \quad (6)$$

In the present systems, $|\chi_{CD}|$ between iBMA and nBMA appears to be considerably large compared to both $|\chi_{AC}|$ and $|\chi_{AD}|$ because miscibility for the PiBMA/PnBMA blend is much more than those for the VC·VAc/PiBMA and Vc·VAc/PnBMA blends except the blend with VC·VAc-97.5. Therefore, if the blend ratio, 1/1, investigated for the present systems is very close to the critical concentration, there may be a possibility of an immiscibility region in the present systems. Then, around the temperature corresponding to the minimum point in the miscibility–immiscibility boundary line, the intermolecular χ changes from negative to positive and again to negative values with the copolymer composition.

Acknowledgment. This work was supported by a Grant-in-Aid for Scientific Research of the Ministry of Education, Science and Culture, Japan (No. 61550654). The authors are grateful to Dr. Y. Tezuka at Nagaoka University of Technology for determination of tacticities with ^{13}C NMR and thank Shin-Etsu Chemical Co., Ltd., for gifts of PVC homopolymers.

Registry No. (VC)(VAc) (copolymer), 9003-22-9; (*n*BMA)-(*i*BMA) (copolymer), 9011-53-4.

References and Notes

(1) Chiou, J. S.; Paul, D. R.; Barlow, J. W. *Polymer* **1982**, *23*, 1543.
(2) Vuković, R.; Karasz, F. E.; MacKnight, W. J. *Polymer* **1983**, *24*, 529.
(3) Kambour, R. P.; Bendler, J. T.; Bopp, R. C. *Macromolecules* **1983**, *16*, 753.
(4) Shiomi, T.; Karasz, F. E.; MacKnight, W. J. *Macromolecules* **1986**, *19*, 2274, 2644.
(5) Paul, D. R.; Barlow, J. W. *Polymer* **1984**, *25*, 487.
(6) ten Brinke, G.; Karasz, F. E.; MacKnight, W. J. *Macromolecules* **1983**, *16*, 1827.
(7) Scott, R. L. *J. Chem. Phys.* **1949**, *17*, 279.
(8) Fernandes, A. C.; Barlow, J. W.; Paul, D. R. *J. Appl. Polym. Sci.* **1986**, *32*, 5481.

Origin of the Long Period and Crystallinity in Quenched Semicrystalline Polymers. 1

E. Robelin-Souffaché and J. Rault*

Physique des Solides, Université Paris-Sud, 91405 Orsay, France. *Received April 1, 1988; Revised Manuscript Received January 31, 1989*

ABSTRACT: The long periods of quenched polymers [in particular linear polyethylene (PE)] of various molecular weight distributions have been determined by small-angle X-ray scattering according to the correlation function, Porod, DAB, and paracrystalline analysis. It is shown that neither of the average molecular weights M_n nor M_w governs the morphology of the semicrystalline state of polymers. The weight-average dimension $r_w \sim M_r^{1/2}$, of the coils in the melted state before crystallization is the main parameter that controls the morphology of the solid state, including long periods, amorphous layer thickness, and crystallinity. This correlation law between the melted and solid states is general, and comparisons between PE, poly(ethylene terephthalate), poly(tetrahydrofuran), and polypropylene are discussed. The role of entanglements during crystallization is clearly analyzed by measurements of the crystallinity $\chi(M_r)$, which is a linear function of $1/r_w$ and which extrapolates to 1 for a molecular weight of the order of M_c, the critical mass between entanglements. Models of crystallizations involving a balance between the enthalpy of crystallization and the energy of distortion of the entangled amorphous chains explain the dependence of the long period and the amorphous layer thickness on supercooling and molecular weight. Finally, the different behavior of amorphous chains of semicrystalline polymers crystallized by slow cooling (relaxed chains) and rapid cooling (constrained chains) is pointed out. The transition between the two regimes of crystallization at high and low supercooling is analyzed in terms of chain dynamics rather than nucleation.

1. Introduction

It is well-known that all properties of bulk-crystallized polymers are drastically dependent on the molecular weight and crystallization temperature.[1,2] The influence of these parameters on the morphology of the semicrystalline state[2-4] and on the kinetics of crystallization[5,6] is well documented. It has been recognized only recently that the morphology on a lower scale, the lamellar arrangment, is also dependent on the molecular weight distribution.[7-16] In monodisperse fractions and mixtures of monodisperse fractions of polyethylene (PE) the long period deduced from the maximum intensity of small-angle X-ray scat-

0024-9297/89/2222-3581$01.50/0

Table I
Characteristics of the Polymers[a]

					I. Monodispersed PE (SNPA)					
10^3M_w		10.5	21.3	31.3	42	60	119.7	236	264	
10^3M_n		9.95	19.4	28.7	38.2	57	112	230	240	
I		1.1	1.1	1.09	1.1	1.05	1.07	1.03	1.1	
					II. Polydispersed PE					
10^3M_w			120	95	143.6		216.6		229.4	
10^3M_n			22	9.6	17.9		21.6		22.9	
I			5.4	9.9	8		10		10	
					III. PTHF					
10^3M_w			37		104.7		500			
10^3M_n			31		95		423.8			
I			1.19		1.1		1.18			
					IV. PET					
10^3M_w	27.8	28.4	32	36.3	42.2	43.7	58.5	67.5		
10^3M_n	12.7	17	16.4	18		22.4		32		
I	2.2	1.67	1.95	2		1.95		2.11		
					V. PP					
10^3M_w	173	206	208	220	262	273	320	332	372	500
10^3M_n	37	37.7	48.5	48.8	48	54	70	69	83	111
I	4.7	5.5	4.3	4.5	5.4	5.1	4.5	4.8	4.5	4.5

[a] M_w and M_n, weight- and number-average molecular weights; I, polydispersity.

tering (SAXS) curves is a linear function of the weight average of the dimension r_w of the coils.[7-9] Using electron microscopy, Voigt-Martin et al.[12-15] have also found that the long spacing in monodisperse PE increases with the molecular weight.

The exact role played by polydispersity in the determination of the properties (morphological and mechanical) of semicrystalline polymers is not understood. No kinetic or thermodynamic theory has predicted the influence of the distribution of the molecular weight, that is, the influence of the different types of average molecular weights (M_n, M_w) on the longer period L, on its fluctuations, or more exactly on the disorder of the lamellar arrangment, and on the crystallinity.

The aim of this work is to show that these parameters are not given by the moments M_n or M_w of the distribution of the molecular weights but rather by a value M_r between M_n and M_w, which is proportional to the square of the weight average of the dimension of the coil in the melted state.

Under SAXS Analysis we compare the long periods and the crystalline layer thicknesses obtained by SAXS measurements using paracrystalline and correlation function analyses. The long periods measured by SAXS are then compared to those obtained by Voigt-Martin et al. by using electron microscopy. It is shown that the correlation between the melted and the solid states observed for weakly polydisperse PE is also valid for highly polydisperse materials and for other semicrystalline polymers. Under crystallinity we show that the crystallinity measured by differential scanning calorimetry (DSC) and by wide-angle X-ray scattering (WAXS) is determined (as L) by the average dimension r_w. The role of entanglements is emphasized. In the next section we show that the crystalline core thickness in semicrystalline polymers, unlike the amorphous layer thickness, is independent of the molecular weight distribution. In the last section we propose a model of crystallization in which the distance between entanglements and the dimensions of the coils in the melted state plays an important role. In this last section we give a new interpretation of the transition between the two regimes (I and II) of crystallization, which is based not on the concept of secondary nucleation theories but on the notion of diffusion-propagated stress on the amorphous chains induced by crystallization.

This paper is principally devoted to linear PE crystallized by quenching, although some comparisons with other semicrystalline materials are given. It will be followed by another paper (part 2), in which we study the morphology of slow-cooled PE and show that in this case the solid and melted states are still correlated.

2. Materials

We report in Table I the number- and weight average molecular weights M_n and M_w, the polydispersity $I = M_w/M_n$, and the weight average r_w of the end-to-end distance of the coils in the melted state. In this ideal state, the unperturbed dimension r_w of the coils is defined by

$$r_w = \sum \omega_i M_i^{1/2} = M_r^{1/2} \quad (1)$$

where ω_i and M_i are the concentration and the mass of species i given by gel permeation chromatography (GPC) and intrinsic viscosity measurements. The end-to-end distance of the PE chain of mass M_i is given by $r_i = 0.95M_i^{1/2} \sim M_i$.[17] The molecular weight average M_r defined by the above relation is a moment of the molecular weight distribution function such that $M_n < M_r < M_w$. The monodisperse PE comes from SNEAP (Société Nationale Elf aquitaine), and the highly polydisperse PE was synthetized by Spitz. Poly(ethylene terephthalate) (PET) was supplied by Rhone-poulenc poly(tetrahydrofuran) and (PTHF) by Polymer Laboratories. These materials have been previously characterized.[7-9] The materials PE, polypropylene (PP), and PTHF had been quenched in water at 20 °C; samples of the same thickness ($e \simeq 1.5$ mm) were sandwiched between aluminum foils. PET was crystallized from the glassy state by annealing 5 min at 160 °C.

The blends of monodisperse PE were made as explained in ref 8. Care was taken to obtain homogeneous blends of high molecular weight polymers. The fractions were dissolved in xylene at 120 °C for 1 h and quenched at 20 °C; the solvent was evaporated and the blends were then melted and annealed at 150 °C for several hours in a silicone oil bath to avoid oxidation and then quenched to room temperature.

3. SAXS Analysis

3.1. Bragg Long Periods of PE. The SAXS intensity curves were obtained at the LURE synchrotron. The beam dimension was 0.3 × 0.3 mm^2 and the distance sample–counter was 2 m. Typical scattering curves obtained with this experimental setup have been given in ref 7. In Figure 1, we give the long periods L deduced from the maximum of the SAXS intensity peak by application of the Bragg law (hereafter called Bragg long period) as a function of

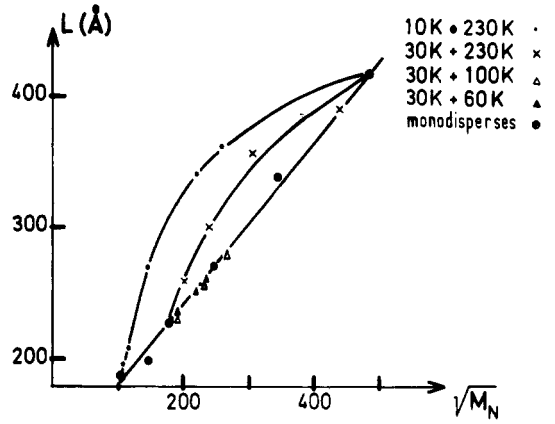

Figure 1. Long periods L of blends of monodisperse PE deduced from the SAXS intensity peak as a function of the square root of the molecular weight M_n (heavy lines) and M_w (dashed lines).

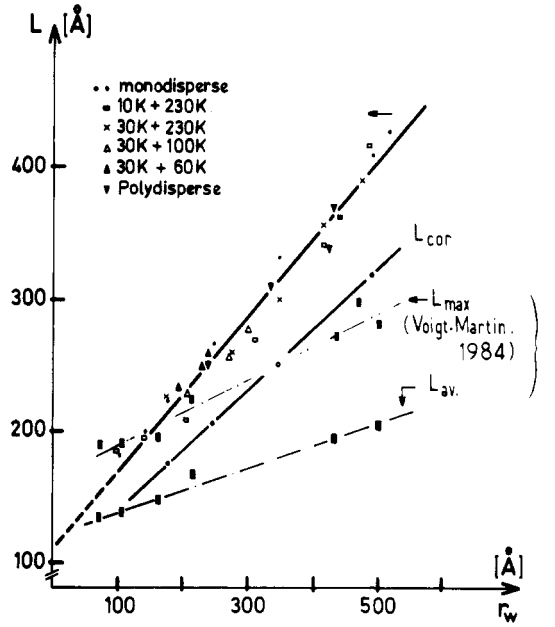

Figure 2. Long periods of quenched PE as a function of the weight-average dimension r_w of the coils in the melted state. The long periods are deduced from the maximum of the SAXS intensity peak L, from the correlation function $K(z)L_{cor}$, and from microscopy studies—L_{max} and L_{av} (after Voigt-Martin et al.[14]).

the square root of the molecular weights M_n and M_w. It is clear from these figures that neither M_n nor M_w is the parameter that controls the long period. Two materials of the same M_n (M_w) but different M_w (M_n) have different long periods. The plateau observed in ref 8 is no longer observed. We think that this is due to the fact that the high molecular weight blends are more homogeneous.

In Figure 2, one recalls the correlation law for polydisperse PE: the Bragg long period L of the semicrystalline state is related to the weight average r_w of the dimension of the coils in the ideal liquid state by the linear relation

$$L = L^0 + \alpha r_w = 117 + 0.56 r_w \qquad (L, r_w \text{ in Å}) \quad (2)$$

where r_w is given by eq 1.

At this stage an important point must be noted. We have reported that for high molecular weight $M > M^* = 10^5$ the long period remains constant. Similar results have been found by Hsiue et al.[10] This is not confirmed by our present results and probably reflects differences in the preparation of the samples: all the present blends were annealed in the melted state longer than the relaxation time defined in ref 7, 10, and 12.

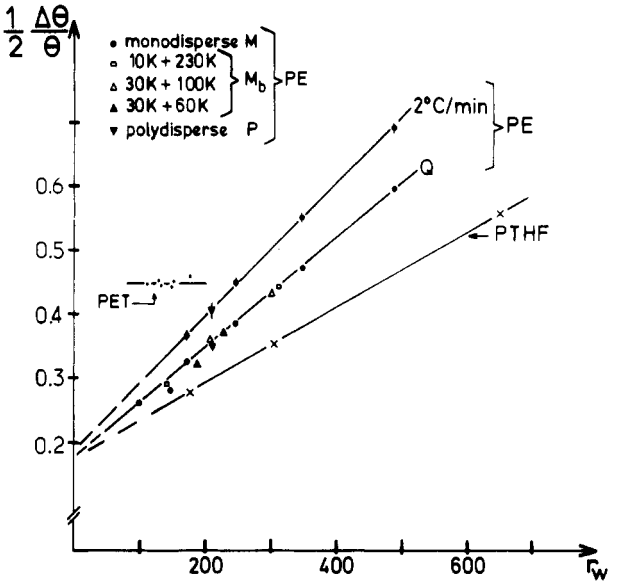

Figure 3. Half-width $^1/_2\Delta\theta/\theta$ of the SAXS intensity peak as a function of the weight-average dimension of the coils r_w for quenched PE and PTHF, slow-cooled (2 °C/min) PE, and PET crystallized from the amorphous state.

The correlation coefficient of this law for the 25 studied samples is 0.96. The master curve $L(r_w)$ must be considered as a calibration curve. Then for a PE of unknown molecular weight, the measure of the Bragg long period L of the sample (crystallized in the same manner as the materials studied here) will give the average molecular weight M_r. The relative accuracy of M_r is in principle equal to the relative accuracy of the long period, which is about 2%. This value is about 1 order of magnitude less than the accuracy in the determination of the molecular weight by GPC. This precision has been obtained with the same experimental setup, using PE of the same molecular weight but of different r_w values, the change of r_w being obtained by changing the melting temperature (see, for example, ref 12). Therefore, the mean deviation of the experimental points from the solid curve of Figure 3 obtained by the least-squares method would be due to the accuracy of the molecular weight distribution determined by GPC and not to the accuracy of the determination of the scattering angle corresponding to the SAXS peak.

Another important point to note is that the shift of the SAXS intensity peak toward a low angle is accompanied by an increase in the relative width of the peak. As noted for L, we did not find any master curve when $\Delta\theta/\theta$ was plotted as a function of M_n or M_w. In Figure 4, we show that the half relative width of the SAXS peak is a linear function of the weight average r_w for quenched and slow cooled PE and for quenched PTHF:

$$\Delta\theta/2\theta = 0.18 + \epsilon r_w \quad (3)$$

The slope ϵ of the curve $\Delta\theta/2\theta$ as a function of $M_r^{1/2}$ is somewhat higher for quenched PE than for quenched PTHF.

In conclusion, the Bragg long period L and the width of the SAXS intensity peak are governed by the same parameter: the weight average of the dimension of the coils. Thus they are governed by the average molecular weight M_r. It is clear from electron microscopy data[13-16] that the morphology becomes less ordered when the molecular weight increases. The simultaneous increase of L and of $\Delta\theta/\theta$ with M_r brings up the classical problem of the interpretation of the maximum of the SAXS peak intensity in the more or less disordered two-phase structure. The measurement of the characteristic dimensions of the do-

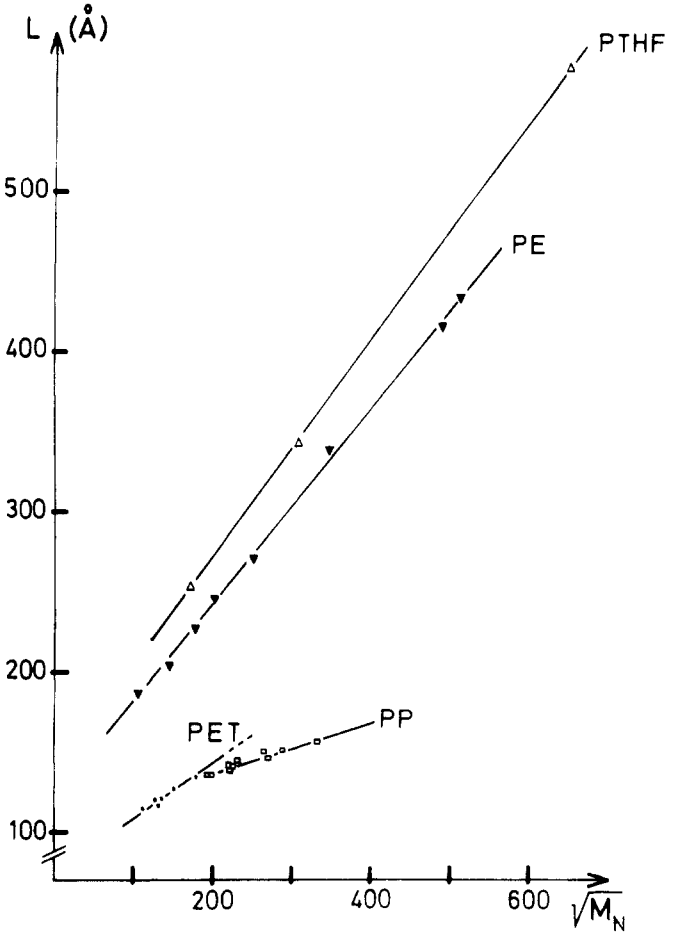

Figure 4. Comparison between the Bragg long period of quenched polymers: monodisperse PE and PTHF and polydisperse PP and PET. PET was crystallized from the glassy state by annealing at 160 °C.

mains can be deduced from the SAXS curve if some assumptions are made on the type of arrangement (one-dimensional lamellar arrangement or heterogeneous random arrangment).

The one-dimensional two-phase structure has been treated by Vonk and Kortleve[18,19] using the correlation function and by Hosemann and Bagghi[20] from the paracrystalline model. In the following sections we apply these analyses for calculating the mean dimensions of the lamellar structure.

3.2. Deviations from the Porod Law. Deviations from the Porod law are due to density fluctuations in the amorphous phase and to the finite thickness e of the interface between crystalline and amorphous layers. The density fluctuations increase with the volume of the amorphous phase and, therefore, with the molecular weight and the temperature. It is important to know if the lamellar arrangement is a perfect two-phase structure with a sharp or a diffuse interface and if the nature and the thickness of that interface depends on the molecular weight distribution.

The generalized Porod law giving the intensity I scattered at large angles is[21-24]

$$\lim_{s\to\infty} I = \frac{K}{s^4}(1 - 4\pi^2 s^2 e^2) + I_b(s) \qquad (4)$$

where s is the scattering vector = $2 \sin \theta/\lambda$, θ the scattering angle, λ the wavelength of the radiation, and e the transition zone thickness. The plot of $I(s)\ s^4$ as a function of s^4 gives the fluidlike component $I_b(s)$. In PE of various molecular weights, the slope of the curve $I(s)s^4$ vs s^4 is constant (obviously proportional to the crystallinity). Therefore, in the studied domain $0 < \theta < 10^{-2}$ rad, for each sample the fluidlike component can be considered as constant. For the Vonk analysis the SAXS intensity curves have, therefore, been corrected for this fluidlike component. It is known that the transition zone thickness can in principle be deduced from the plot $(I(s) - I_b)s^4$ vs s^2. The values of the thickness e of the transition zone are found to be of the order of 5 Å, which is about the accuracy of the measurements, owing to the statistics of the counts measured on the linear counter and to the finite angular domain studied. In conclusion, the interface in linear PE can be considered as sharp and not dependent on the molecular weight. Important transition zones ($e \sim$ 10–20 Å) have been found only in low-density PE[18,19,26] and in segregated block copolymers and blends.

It is important to note that a sharp change in the electron profile across the crystal–amorphous boundary layers does not mean that there is no density gradient between the two phases. Transition layers are not ruled out by the present Porod analysis. In a following section we will show that the sharpness of the crystal–amorphous boundary is confirmed by the behavior of the correlation function $\gamma(z)$ near the origin.

3.3. Correlation Function Analysis (Strobl Analysis 26). The analysis of the SAXS intensity curve based upon the one-dimensional electron-density correlation function has been given by Vonk and Kortleve.[18,19] These authors calculated the experimental correlation function as

$$\gamma(z) = \int_0^\alpha s^2 I(s) \cos 2\pi sz \, ds \Big/ \int_0^\alpha s^2 I(s)\, ds \qquad (5)$$

$I(s)$ is the experimental SAXS intensity corrected for thermal fluctuations. These authors have compared this experimental function to the theoretical one of a one-dimensional arrangment with various distribution functions for the amorphous and crystalline layers. Strobl et al.[26] do not fit the experimental correlation function with that of a theoretical model. They analyzed directly the experimental curve $K(z)$

$$K(z) = \gamma(z) \int_0^\infty s^2 I(s)\, ds \qquad (6)$$

in order to deduce the different morphological parameters of the structure. This procedure is relevant because for PE with a high degree of crystallinity ($x > 0.5$), the choice of distribution functions is not important. In the above relation the intensity $I(s)$ has been corrected for background scattering due to the fluidlike amorphous phase.

In this work, we use the procedure of Strobl et al. for determining the long period L_{cor} and the crystalline core thickness l_{cor}. The long period L_{cor}, deduced from the first maximum of the correlation function $K(z)$, denotes the most probable long spacing. The crystalline core thickness l_{c3r} is given by

$$l_{cor} = \frac{Q}{\chi} \frac{dK(z)}{dz}, \qquad \text{for } 0.5 < \chi < 1 \qquad (7)$$

where Q is the integrated intensity and χ the crystallinity measured by DSC. In the domain of crystallinity studied here, $0.3 < \chi < 0.7$, the crystalline core thickness cannot be directly deduced from the correlation curve, and another technique is necessary for determining χ.

The Porod law observed in this domain is extrapolated up to $4s_{max}$ ($s_{max} \sim 1.6 \times 10^{-2}$ Å^{-1}). At low angles, $s < s_{min}$ ($s_{min} = 8 \times 10^{-4}$ Å^{-1}), different extrapolations have been performed, and as noted by Vonk and Kortleve and by

Strobl et al., these have no influence on the correlation function.

In Figure 2 we report the variation of L_{cor} with $M^{1/2}$ for monodisperse PE. The relation

$$L_{cor} = L^0_{cor} + \alpha r_w = 94 + 0.46 r_w \quad (8)$$

found for monodisperse PE is also verified for polydisperse PE. The slope of the curve for $L_{cor}(r_w)$ is somewhat lower than that of $L(r_w)$ given by eq 2. Equations 3 and 8 give the relation between L, L_{cor}, and $\Delta\theta/\theta$:

$$L_{cor} = L - K\Delta\theta/2\theta \quad (9)$$

with $K \simeq 156$ Å, independent of the molecular weight. This relation shows that the difference between the two long periods L and L_{cor} is a measure of the disorder of the lamellar arrangement. It has been shown that the same relation applies for preoriented PET yarn crystallized from the glassy state.[32]

It is important to note that for all the PE materials $10\,000 < M_r < 230\,000$) the correlation function $K(z)$ near the origin shows very weak curvature, indicating that the transition zone between the two phases is very sharp (as shown by the Porod analysis). Using Strobl analysis, the disorder of the two-phase structure cannot be directly deduced in a straightforward manner from the experimental $K(z)$ curve. This parameter is analyzed in detail in the paracrystalline analysis.

3.4. Paracrystalline Analysis. Let us assume that the long period of a lemallar arrangment is given as a functional probability $P(L)$ and that the mean value $\bar{L}$ is constant (independent of M). When the width $\bar{\Delta L}$ of the distribution function increases, the SAXS intensity peak is shifted to low angles and the long period L deduced from the peak maximum increases, whereas the mean long period $\bar{L}$ is constant. This effect has been studied by several authors (see for example ref 27–30). Looking at the experimental results of Figures 2 and 3, one may ask if the increase of L with r_w is a consequence of the increase of the disorder. In the paracrystalline model the relationship between the true long period L_p, the Bragg long period L, and the relative width $\Delta\theta/\theta$ of the SAXS peak has the form

$$\frac{L}{L_p} = K_0 + K\frac{\Delta\theta}{\theta} \quad (10)$$

in the domain of important fluctuations $0.2 < \Delta\theta/\theta < 1$. The constants $K_0 \sim 1$ and $K \sim 0.2$ do not vary significantly with the form of the distribution functions $P(l_c)$ and $P(l_a)$ of the crystalline and amorphous layers thicknesses. This relation, obtained first by Tvanskin, has been discussed by several authors (see, for example, ref 28). Reckinger et al.[30-31] deduced the same relation for paracrystalline models with bimodal distribution. Slutsker,[29] using light scattering on a paracrystalline arrangement printed on a photographic plate, arrived at the same conclusion. This author found that the relative width of the light intensity peak scattered at low angles is given by the relation

$$\Delta L/L = 0.06 + 0.55\Delta\theta/\theta \quad (11)$$

where $\Delta L/L$ is the relative function of the long period of the paracrystalline arrangement. Equation 11 is nearly identical with eq 10 if one assumes that $\Delta L/L \simeq (L - L_p)/L_p$. By putting into eq 10 the experimental values of L and $\Delta\theta/\theta$, both functions of r_w (eq 2 and 3), one obtains the relationship between L_p and r_w:

$$L_p = L^0_p + \alpha r_w = 120 + 0.45 r_w \quad (12)$$

The application of the calibration curve of Slutsker gives a similar relation.

In summary the long periods deduced from the correlation functions and from the paracrystalline model are of the same order of magnitude and present similar variations with the molecular weight M_r. These two analyses are based on the same assumption, that the lamellar arrangment is one-dimensional. This assumption breaks down when the width of the lamellae become comparable to the long period. When the molecular weight increases, the lamellae becomes curved and the arrangment consequently becomes less ordered and loses somewhat its one-dimensional character. For $M \geq 2 \times 10^5$, the Debye et al. analysis becomes applicable.[21] This analysis applied to heterogeneous and random two-phase systems is not discussed here. Although the exact SAXS analysis of high molecular weight PE is far from complete, the one-dimensional model is generally accepted when the lateral size and the curvature radius of the crystalline lamellae are much greater than the long period.

Finally, we give in Figure 2 the results of Voigt-Martin et al.[14-16] obtained by transmission electron microscopy (TEM) for the long periods L_{max} and L_{av} of quenched monodisperse PE, where L_{max} is the maximum of the long period and L_{av} the average value of the distribution $P(L)$ measured from electron micrographs. The exact mathematical definition of these long periods has not been given, although the authors claim that these parameters are number averages instead of weight averages. This could explain why these long periods are shorter than those measured by X-ray. The important point to note is that here again L_{max} and L_{av} are linear functions of r_w ($\sim M_r^{1/2}$).

In conclusion, the exact mathematical description of the lamellar arrangment is difficult to achieve, but the one-dimensional model seems to be a useful approximation of the structure. The long periods measured by X-ray (L, L_{cor}, L_p) and by electron microscopy (L_{max}, L_{av}), corresponding to different values of the distribution function of the long period, show the same dependence on the molecular weight M_r. One important feature is that the ordinates at the origin of the curves $LM_r^{1/2}$, $L_{cor}M$, and L_pM have the same value (which is about the crystalline layer thickness l_c)9 Obviously, when the value of M_r decreases, the arrangment becomes more perfect, the distribution of the long periods becomes sharper, and the difference between the various moments (L, L_p, L_{cor}) of the distribution $P(L)$ decreases.

3.5. Comparison between PE and the Other Semicrystalline Polymers. We compare in Figure 4 the Bragg long periods of PTHF, PP, and PET with those of monodisperse PE as a function of $M_n^{1/2}$. The comparison between PTHF and PE is particularly interesting. In Figure 3 we show that for both types of quenched polymers, the disorder expressed by the parameter $\Delta\theta/\theta$ increases linearly with $M_r^{1/2}$ and consequently with $M_n^{1/2}$ for monodisperse polymers. The disorder is somewhat lower for PTHF than for PE for an equivalent molecular weight. The application of the correlation function analysis to the monodisperse PTHF gives the long period L_{cor}(Å):

$$L_{cor}(\text{PTHF}) = 106 + 0.52 M_n^{1/2} \quad \text{(cf. eq 8 for PE)} \quad (13)$$

The application of a paracrystalline model gives similar results; L_p for PTHF is again a linear function of $M_r^{1/2}$ and the slope of the curve for $L_p(M_r^{1/2})$ is of the same order of magnitude as that of the PE sample.

PE and PTHF obey a similar relation with nearly the same coefficient, because both polymers have similar rigidity C:[17b]

$$C = r^2/Na^2 \quad (14)$$

where r is the end-to-end distance of a chain of N skeletal

bonds of length a. The experimental values for C^{33} for PE and PTHF are respectively 6.4 and 6. Conformational calculations by Geny[34] indicate that the radii of gyration of the coils of these two polymers in the melted state differ only by a factor 1.1.

The same behavior is observed for highly polydisperse PP. A linear increase of L with the number-average molecular weight is noted in the small range of molecular weight studied here. For the same molecular weight of PE and PP, the ratio of the number of skeletal bonds N(PE)N(PP) is 1.5. The ratio of the rigidities C(PE)/C(PP) is 1.17 according to Flory,[17b] therefore the ratio of the end-to-end distances is r(PE)/r(PP) $\sim$ 1.3. This is smaller than the mean value observed for the ratio of the long periods L(PE)/L(PP) $\simeq$ 2. This large difference between the two ratios is rather puzzling. We emphasize, however, that it is difficult to make a comparison between the molecular weights of two different polymers. The determination of the molecular weight by GPC requires a high degree of solubility of the materials in a solvent. For PE and PP the solvent and the temperature during permeation in the GPC column are not the same, so the dimensions of the coils of PE and PP with the same number of skeletal bonds can be very different.

The comparison between PE and PET is interesting because these polymers have been isothermally crystallized from the melted state and from the glassy state, respectively. In PET the relative width of the SAXS peak intensity is constant, the L_{cor} values are lower than the Bragg values, and the slopes of the curves L and L_{cor} vs $M^{1/2}$ are the same. The difference in the absolute value of L (and of L_{cor}) between PE and PET has been related to the difference in dynamic rigidity of these two polymers and not to the static rigidity.[9]

In conclusion, the linear relation between L and L_{cor} vs $M^{1/2}$ in isotropic semicrystalline polymers is general and is observed for any cooling rate.[36] In ref 32 we given one exception to that law. It is observed in preoriented amorphous PET obtained by spinning that crystallization above T_g gives rise to a lamellar structure with Bragg long periods independent of the molecular weight. The difference in the scaling laws $L \sim M^{1/2}$ and $L \sim M^0$ observed in isotropic and oriented (or preoriented) materials clearly indicates that the process of crystallization is different for these two materials.

For oriented materials it has been proposed that the process of crystallization is similar to the spinodal decomposition,[35] where the mean distance between segregated domains is not dependent on the length of the chains.

4. Crystallinity

The influence of molecular weight on the crystallinity of PE was first noted by Richards[37] and Burch et al.[38] Recently, Mandelkern et al.[2,3] measured the crystallinity of monodisperse ($27\,000 < M < 250\,000$) and polydisperse ($418\,000 < M < 6 \times 10^5$) PE; however, the type of average molecular weight that controls the crystallinity cannot be determined from their data because for high molecular weight materials only the viscosity molecular weight M_η was known and for low molecular weight only fractions were used.

The crystallinity χ was measured by DSC at a heating rate of 10 °C/min and by WAXS according to the Wakelin method.[39-42] This last method gives an index of crystallinity that is proportional to the DSC crystallinity and proportional to the absolute value of the crystallinity measured by the Ruland method.[24] The index of crystallinity determined by the Wakelin method depends on the standard crystalline and amorphous reference materials. The standard crystalline reference material is a PE obtained by extrusion at high pressure. This material of crystallinity $\chi \simeq 1$ has been randomized according to the mechanical method of Sotton et al.[42] The amorphous standard reference material is the molten state, and the WAXS intensity curve of this sample has been extrapolated to room temperature, knowing the thermal dilatation coefficient of the melt state. The χ values of these reference materials obtained by the Wakelin method are in good agreement with those obtained by DSC. The reproducibility of both methods is about 1%. For the following, the reproducibility of the measurements is much more important than the accuracy of the absolute values. We are essentially interested here in the variation of χ as a function of the molecular weight.

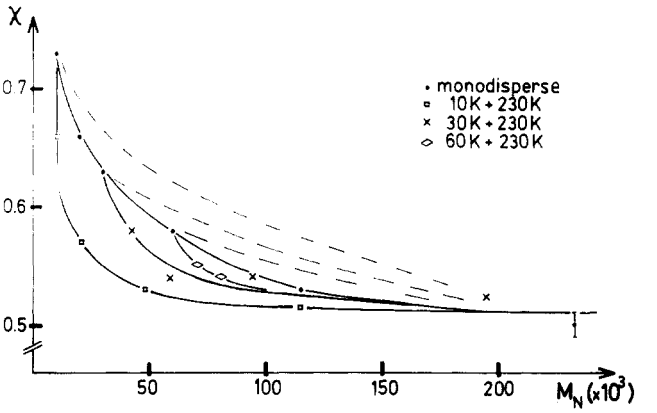

Figure 5. Crystallinity χ of blends of monodisperse PE as a function of the molecular weight averages M_n. A similar set of curves is observed when χ is plotted versus M_w (dashed lines).

In Figure 5 we give the crystallinity measured by DSC of PE fractions and mixtures of fractions as a function of M_n. Similar curves are obtained (in dashed lines) when χ is plotted as a function of M_w. No master curve is obtained either for $\chi(M_n)$ or for $\chi(M_w)$. In other words, different PEs having the same M_n (or M_w) values but different M_w (or M_n) values do not have the same crystallinity. It should be noted that the scatter of the points cannot be explained by the accuracy of the measurement of χ. We point out that the value of χ for a monodisperse material of molecular weight M is higher (or lower) than that of a polydisperse one having a weight-average (or a number-average) molecular weight equal to M. Obviously the molecular weight that governs the crystallinity is a moment of the distribution function intermediate in value between the moments M_n and M_w. As the long period L (and L_{cor}) is given by the moment M_r, one expects that this moment governs also the crystallinity.

The linear crystallinity (l_c/L) is inversely proportional to the long period and therefore to the weight average of the dimension of the coils r_w, if ones admits that l_c is independent of r_w (see next section). In Figure 6 we show the crystallinity measured by DSC and by WAXS as function of $1/r_w$. It is important to remark that monodisperse, mixtures of monodisperse and highly polydisperse materials obey the experimental law

$$\chi = 1 - \psi\left(\frac{1}{r_c} - \frac{1}{r_w}\right) \qquad (15a)$$

The constants ψ and r_c are different for quenched and slow-cooled materials. The scatter in the experimental points does not seem to depend on the polydispersity. Nearly the same correlation coefficients (0.95 and 0.93) of the linear regresson $\chi(1/r_w)$ are obtained for polydisperse

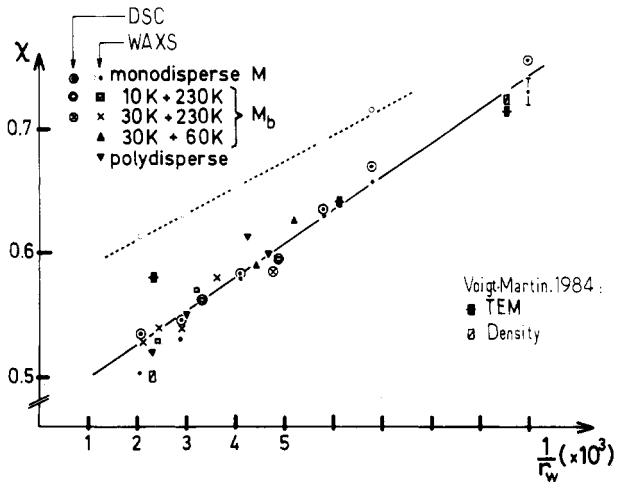

Figure 6. Crystallinity χ of quenched PE as a function of the inverse of the average dimension r_w of the coils in the melted state. The rectanles represent the values determined by Voigt-Martin et al. by transmission electron microscopy (TEM) and by density.[13] The dashed line represents the values of χ for slow-cooled PE (10 °C/min).

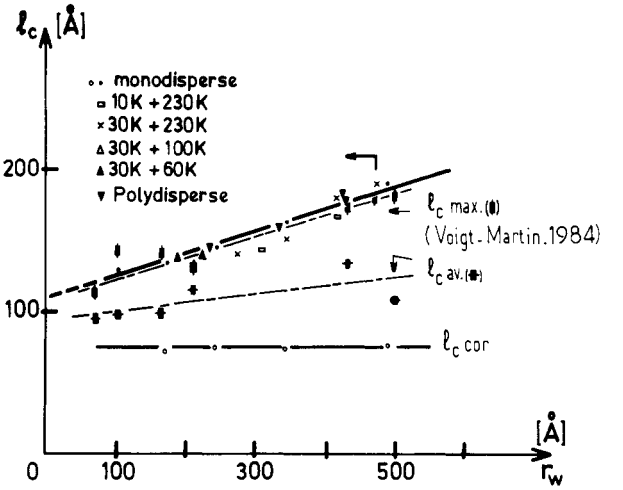

Figure 7. Crystalline layer thickness of quenched PE as a function of the weight-average dimension of the coils r_w; l_c is deduced from the values of L (Bragg long periods) and the crystallinity χ; l_{cor} is deduced from the correlation function $K(z)$ and from χ; $l_c(max)$ and $l_c(av)$ are the values determined by Voigt-Martin et al. by electron microscopy.[14,16]

and monodisperse materials. When plotted as a function of L_{cor}, χ obeys the experimental law

$$\chi = 0.4 + 51/L_{cor} \tag{15b}$$

From Figure 6 and eq 15, one draws the anticipated conclusion that the crystallinity in the domain $10^4 \leq M_r \leq 2.5 \times 10^5$ is determined by the moment M_r of the molecular weight distribution. Another important conclusion concerns the role of entanglement in the process of crystallization: the extrapolated values r_c and r_w, which lead to a crystallinity $\chi = 1$, are 53 and 48 Å, respectively, for quenched and slow-cooled materials, 10 °C/min. This value is approximately equal to the mean distance $r_c = M_c^{1/2}$ between two entanglements in the melted state, the critical mass M_c between entanglements being of the order of 1900 for polyethylene.[43]

In conclusion, in semicrystalline polymers the existence of the amorphous phase is due to entanglements in the melted state. The morphology of a semicrystalline polymer is obviously dependent on the degree of entanglement in the melted state before crystallization. In these biphase systems, it still remains to identify which factors determine the thickness of both domains. Up to now, no attempt has been made to explain either the origin of the amorphous phase or the origin of the finite crystallinity of semicrystalline polymers.

5. Thickness of the Crystalline and Amorphous Layers

5.1. Crystalline Core Thickness of PE. We show in Figure 7 the crystalline core thicknesses l_c and l_{cor}. The value of the core thickness l_c is deduced from the long period L and from the crystallinity χ by the relation

$$l_c = \chi \frac{L\rho_a}{\rho_c - \chi\Delta\rho} \tag{16}$$

where ρ_c and ρ_a are the crystalline and amorphous densities and $\Delta\rho = \rho_c - \rho_a$. The value of l_{cor} is deduced from eq 7.

The crystalline core thicknesses of polydispersed PE obey the relations

$$l_c = l^0{}_c + \beta r_w = 101 + 0.18 r_w \tag{17}$$

and $l_{cor} = 73$ Å.

The value of l_c deduced from the Bragg long period is obviously overestimated. The important point to note is that the increase of l_c with r_w is lower than that of L (and L_{cor}) and that this increase is due essentially to the increase in the relative width of the SAXS peak. In the same figure are shown the values of Voigt-Martin et al. obtained by electron microscopy of monodisperse PE stained with OsO_4 (from Table II of reference 15). These authors, by analyzing the histograms, found that the crystalline core thickness has a broad distribution ($\Delta l_c/l_c \simeq 0.5$). They have defined an average value $l_c(av)$ and an upper limit $l_c(max)$ of the measured values of the crystalline core thickness. The rigorous mathematical definitions of $l_c(av)$ and $l_c(max)$ were not given; however, by comparing these values with the distribution function of l_c given by the histograms $P(l_c)$, one can say that $l_c(av)$ is approximately equal to the most probable value or the number-average value of $P(l_c)$ and that $l_c(max)$ is a weight average. Whereas the mean value $l_c(av)$ is constant, the width of the distribution $P(l_c)$, measured by the difference $l_c(av) - l_c(max)$, increases with molecular weight. This same conclusion is drawn from our X-ray measurements. The mean value l_{cor}, which is a most probable value of $P(l_c)$, is constant, whereas the Bragg value l_c, which is very sensitive to the width of the distribution $P(l_c)$, increases with the molecular weight.

In summary, from electron microscopy and SAXS measurements, one can conclude the following: (a) The mean crystalline thickness l_{cor} corresponding to the most probable value is independent of molecular weight. (b) The disorder of the structure increases with molecular weight. The width of the distribution $P(l_c)$ of the crystalline lamellar thickness increases linearly with $M^{1/2}$. The same conclusion is drawn from the distribution of the long period $P(L)$. (c) The values of l_c and l_{cor} determined by SAXS and WAXS, which involve a certain number of assumptions, are of the same order of magnitude as the values $l_c(max)$ and $l_c(av)$ determined by electron microscopy.

Raman studies of the low-frequency LAM mode show that the stem length l_c is more or less independent of the molecular weight distribution.[45,59] A systematic study of the stem length as a function of the molecular weight distribution using this direct technique would ould be interesting because of its high accuracy. However, in light of results already published and of our work, no great change is expected in the values of l_c with the molecular weight distribution.

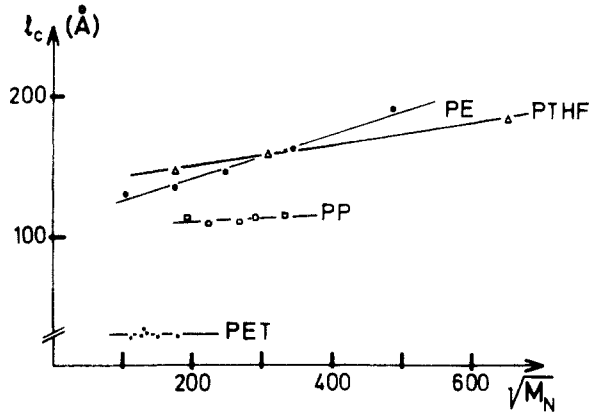

Figure 8. Comparison between the crystalline layer thickness l_c of PE, PTHF, PP, and PET.

5.2. Comparison between the Crystalline Core Thickness of the Different Semicrystalline Polymers. In Figure 8 we compare the l_c values of PE, PTHF, PP, and PET as a function of molecular weight; the comparison between the different polymers permits one to conclude that the increase of l_c with $M^{1/2}$ (when observed) is correlated to the increase of disorder of the structure with $M^{1/2}$. The same conclusion was also reached in the preceding section concerning PE. We make the following remarks concerning Figure 8: (a) Polymers of similar nature (similar rigidity) and crystallized in the same way, like PE and PTHF, have similar l_c (and l_{cor}) values. The disorder (as represented by the relative $\Delta\theta/\theta$) of PTHF increases slower with $M^{1/2}$ than that of PE, consequently the increase of l_c with $M^{1/2}$ is lower for the former polymer. (b) PET crystallized from the glassy state and PP crystallized from the melted state each have a degree of disorder (that is to say a $\Delta\theta/\theta$ value) that does not vary with molecular weight; consequently the crystalline core thickness l_c of each of these polymers is independent of molecular weight. It is important to note that for PET, l_c can be measured directly by WAXS from the width of the ($\bar{1}05$) reflection; such measurements of l_c are independent of M.

In conclusion, the l_{cor} value of a semicrystalline polymer (as opposed to the long period) is an intrinsic parameter of the chain, which does not depend on the molecular weight. The small increase in the value of l_c with M is only due to the increase of disorder of the lamellar structure with molecular weight.

5.3. Thickness l_a of the Amorphous Phase. One postulates that the distributions of thicknesses $P(l_c)$ and $P(l_a)$ of the crystalline and amorphous layers are independent, assuming no correlation between two adjacent layers (amorphous and crystalline). Therefore, one can deduce l_a from the Bragg parameters L and l_c or from the dimensions L_{cor} and l_{cor} by the relations

$$l_a = L - l_c \tag{18}$$

and

$$l_a = L_{cor} - l_{cor}$$

In Figure 9 we show the amorphous layer thickness l_a as a function of the square root of the molecular weight for monodisperse PE. The two different measurements of l_a give very similar results, and l_a is found to obey the linear relation

$$l_a = l^0_a + \gamma M^{1/2} \tag{19}$$

where $l^0_a \simeq 12$ Å and $\gamma = 0.44$. The slopes α and γ of the curves $L(M^{1/2})$, $L_{cor}(M^{1/2})$, and $l_a(M^{1/2})$ are equal. The

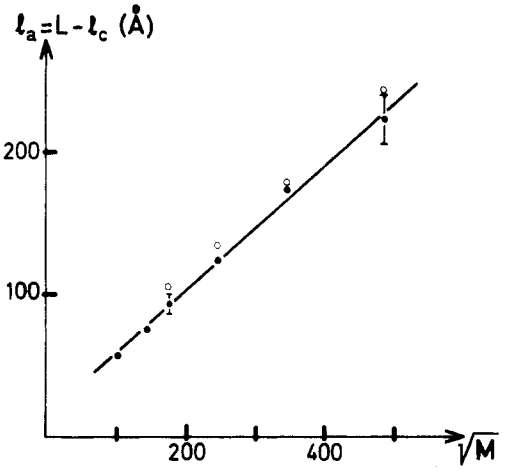

Figure 9. Amorphous layer thickness l_a of quenched PE as a function of the square root of the molecular weight for monodisperse polymers; l_a is deduced from crystallinity measurements and from either the Bragg long period (●) or the long period L_{cor}, and the crystalline layer thickness l_{cor} is deduced from the correlation function (○).

same relation is obtained for polydisperse PE, but as already pointed out, M in the above relation is replaced by the average value M_r. Here we emphasize that the average values of l_a determined from the Bragg long period and the correlation long period should in principle be different. The fact that these two values are equal (for the same molecular weight) has no straightforward explanation. It should be point out that if both L and l_c are obviously overestimated to the same degree, the difference $L - l_c$ could approach the real value.

Despite the systematic errors in the values of L, L_{cor}, l_c, and l_{cor}, the relation given by eq 19 is of interest, not for the determination of the absolute value of the amorphous layer thickness but rather for its relative variation with molecular weight. For low molecular weight materials ($M < M_c$) the value of l_a extrapolates to zero, as expected. Oligomers of molecular weight smaller than M_c are fully extended in the crystalline state, and the crystallinity $\chi \simeq 1$ does not vary conspicuously with molecular weight. Equation 19 applies also for the other semicrystalline polymers. The l_a values of PTHF fit the same curve $l_a(M^{1/2})$ drawn in Figure 9 for PE but are not reported in the figure to preserve clarity.

For PET, the curve $l_a(M^{1/2})$ deduced from the correlation function is also linear ($l^0_a = 34$ Å and $\gamma = 0.19$ in eq 19). As pointed out in sections 3.5 and 5.2, this polymer is especially interesting because the crystalline core thickness l_c can be determined directly from WAXS. For this polymer the measurements of l_c and l_a do not involve the same assumptions required for PE and PTHF, which lead to eq 16.

Whether the polymer is crystallized from the melted or from the glassy state, the scaling law giving the amorphous layer thickness versus the molecular weight is the same. This conclusion suggests that the linear form $L \sim L_{cor} \sim L^0 + \alpha M^{1/2}$ is valid whatever the cooling rate. This will be verified in paper 2.[36]

6. Discussion

The fact that the crystalline and amorphous layer thicknesses scale differently with molecular weight (respectively M^0 and $M^{1/2}$) indicates that there are two different and independent mechanisms that govern the morphology of semicrystalline polymers. Up to now, most of the experimental and theoretical work on crystallization of polymers has been devoted to the crystalline lamellar

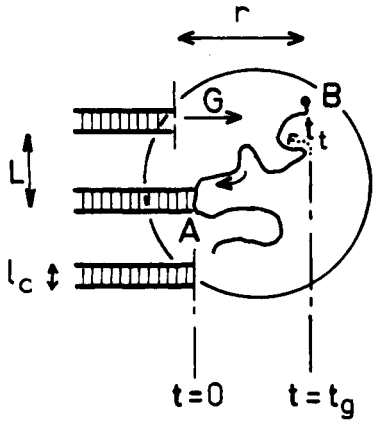

Figure 10. Characteristic time envolved in the process of crystallization. A Gaussian chain of dimension r is trapped by two crystalline lamellae. The chain crystallizes first in A and then in B after an average time t_g has elapsed. During crystallization in A, the reeling-in process produces a stress (and then a displacement of the chain) that propagates along the chain and arrives in B at a time t_t.

thickness and its variation with supercooling. Little attention has been paid to the variation of the amorphous layer thickness. For a given molecular weight and a given supercooling (or cooling rate), one must ask what is the main parameter and the physical mechanism that limits the crystallization and therefore the crystallinity? The aim of this section is to propose a mechanism of crystallization in which the entanglements and the deformation of the amorphous chains play an important role.

The starting point is the well-known identity between the radius of gyration of the coils in the melted and in the quenched solid state[46-49] and the identity $L \sim r$ reported here. SAXS and neutron scattering experiments indicate clearly that cold crystallization (crystallization at high supercooling) involves rearrangement of only part of the chains. Obviously, the entanglement network existing in the melted state (or in the glassy state) does not disappear during fast crystallization.

6.1. Description of the Two Regimes of Crystallization. It is obvious that for slow crystallization from the melted state, or from solution, the amorphous chains stay in the ideal configuration when a portion of the chain crystallizes; in other words, the melted phase around a crystallite maintains its equilibrium structure. During slow crystallization, chains disentangle in such a way that the concentration of entanglements in the amorphous phase stays constant. The effect of chain segregation in polydispersed polymers and in blends during crystallization at low supercooling is a clear indication that chains disentangle.[66-70] At high supercooling the entanglements are trapped and one asks then what is the critical supercooling rate that separates these two domains? The following analysis is different from those advanced by Yoon and Flory[49] and by Hoffman et al.[72]

In the first domain each lamella crystallizes independently, while in the second, adjacent crystallites are coupled by strained amorphous chains. One can visualize this transition between the two regimes from the following arguments (see Figure 10).

During crystallization a chain is pulled from the amorphous phase; however, as described by de Gennes,[71] this phenomenon is not instantaneous, and the tension induced in the tail by the growing stem extends up to a number of monomers $n(t)$ along the chain:

$$n(t) \sim (\nu_0 t)^{1/2} \tag{20a}$$

where $\nu_0 \sim 10^9\ s^{-1}$ is the jump frequency between rotational isomers (see for example ref 73-74) and t the elapsed time since the beginning of crystallization of the stem. This tension propagates along the chain and is finally exerted on the whole chain at the time

$$t_t = N^2/\nu_0 \tag{20b}$$

Let us consider now a second lamella crystallizing at a distance $L \simeq r$ from the first one; these two lamellae belong to the same spherulite and have the same growth rate. The chain crystallizing in lamella A will be trapped by the adjacent crystallite B if the time t_g

$$t_g = r/G \tag{21}$$

where G is the growth rate, is smaller than the time t_t. In this case, tie molecules connecting adjacent lamellae are numerous. In the opposite case $t_g > t_t$, the chains have time to relax, and the crystalline lamellae remain independent.

Essentially the difference between the two regimes is that the amorphous chains linking two lamellae are in an equilibrium state in regime 1 and in a nonequilibrium state in regime 2. The same difference would exist in the concentration of entanglements in the amorphous layers. It is obvious that the kinetics of crystallization and the morphology in these two regimes are different; however, this will be analyzed in a subsequent paper. The critical temperature T^*, which separates the two regimes, is given by the relation $t_g = t_t$, which gives

$$G = r\nu_0/N^2 \tag{22}$$

For PE, $\nu_0 \simeq 10^9$–$10^{10}\ s^{-1}$ and $r = 0.95M^{1/2} \simeq 3.4N^{1/2}$ Å. For any molecular weight, G can be written in the form

$$G = G_0 \times 10^{(T_0-T)} \tag{23}$$

according to results of Hoffman et al.[5,51,52] (see in particular Figure 3 of ref 52).

For the (arbitrary) reference temperature $T_0 = 129$ °C and for $M = 18000$, we find that $G_0 \sim 10^{-8}$ cm/s = 1 Å/s.

Equations 22 and 23 give

$$10^{T_0-T^*} = \frac{3.4}{N^{3/2}}\frac{\nu_0}{G_0} \simeq \frac{3}{N^{3/2}}10^9 \tag{24}$$

For the molecular weight $M = 18000$, the critical temperature T^* is in degrees Celsius

$$T^* = 120 + \tfrac{3}{2}\log N \simeq 125\ °C \tag{25}$$

which is exactly the measured value that separates the two regimes. The exact dependence of T^* on the molecular weight, predicted by eq 22 and 24, is determined by the dependence of G on M in the first domain. According to the results of ref 70, $G_0 \sim (M)^x$ where $1 < x \leq {}^3/_2$. Therefore, the dependence of T^* on the molecular weight given by eq 24 is

$$T^* \sim (\tfrac{3}{2} + x)\log N \sim 3 \log N \tag{26}$$

This predicts that an increase in M by a factor of 3 increases the temperature T^* by 1.4 °C. This is observed, experimentally, when comparing the T^* values of PE fractions of molecular weight 74 000 and 30 000 with the same polydispersity.[52] The effect of the polydispersity on T^* will be analyzed elsehwere.

In conclusion the criterion expressed by eq 22 gives the value of the critical temperature T^* separating the two different regimes of crystallization and its variation with molecular weight.

The interest of this analysis is that it is not based on definitions of the surface free energy and of supercooling

(the exact value of the equilibrium melting temperature T_m^0). In part 2 it is shown that the temperature of crystallization of quenched PE (~120 °C) does not vary significantly with the cooling rate (for cooling rates higher than 5 °C/min). This temperature is about 5 °C below the critical temperature T^*. In quenched PE, the regime of crystallization is obviously regime 2, where the tension time t_t is greater than the growth time t_g. In quenched PE the chains are obviously trapped by adjacent lamellae. The effect of molecules which crystallize at two (or more) different places is to slow down the growth rate. The chains, called tie molecular, are not in their equilibrium configuration and the entanglements are trapped in the amorphous phase. These two effects can explain the correlation law $L \sim r$ and the finite crystallinity observed in semicrystalline polymers. But before discussing these effects and the origin of the long period, we turn to the physical process that explains the dependence of the crystalline core thickness l_c on supercooling.

6.2. Origin of the Crystalline Core Thickness. A great deal of theoretical and experimental work has been devoted to the role of secondary nucleation on the limitation of the thickness l_c of crystalline lamellae crystallized from the melted state and from solution (see, for example, ref 50). The limitation of l_c at high supercooling has also been explained by several authors (Rault,[5,56] Point,[57] and Allegra[58]). All of these models rest on the fact that the Gaussian chain, when crystallizing from solution or from the melted state onto a crystalline face, has a certain probability P_F of folding back onto the surface or into the bulk. The probability P_F is obviously a decreasing function of the rigidity C of the chain. The folding of the chain in the crystalline state would be an image of the folding of the chain in the liquid state just before crystallization. All of these theories and models explain the independence on l_c of the molecular weight distribution. The results reported in this paper (Figure 10) indicate that the value of l_c is an increasing function of the rigidity C of the chain in the liquid state. The same conclusion was reached when comparing values of l_c for polymers of different nature crystallized from solution (see Figures 6–10 of ref 55) and for PE crystallized from the melted state by quenching at different temperatures.[59,60] It should be mentioned that the limitation of l_c can have several origins. Posthuma de Boer and Pennings[63] have shown the effect of cross-links on the values of l_c in isotropic and stretched networks. In melted crystallized polymers, the effect of entanglements could also be invoked;[7] however, this is still a subject of debate, and the role of entanglements is not yet clear. We emphasize that the different processes of crystallization quoted above cannot explain the dependence of the long period and of the amorphous layer thickness on the molecular weight distribution.

6.3. Origin of the Long Period and of the Amorphous Layer. We discuss separately the trapping of entanglements and the deformation of the amorphous chains. Both phenomena, leading to a nonequilibrium amorphous phase, are, however, not independent if one admits that the degree of entanglement depends on the configuration of the amorphous chains.[61,62]

(a) Effect of Entanglements. If we assume that the crystalline core thickness l_c is fixed by the process of crystallization (nucleation theories, fold defects and loops along the liquid chain, presence of entanglements), we then ask what process limits the long period, i.e., the amorphous layer thickness.

It is obvious that when two crystalline lamellae are formed, the amorphous phase between them can relax if their separation is greater than the mean dimension of the chains. In that case new lamellae can crystallize in the unperturbed amorphous phase. The phenomenon of interlamellae crystallization is well documented[26,31,64,65] (Figure 11).

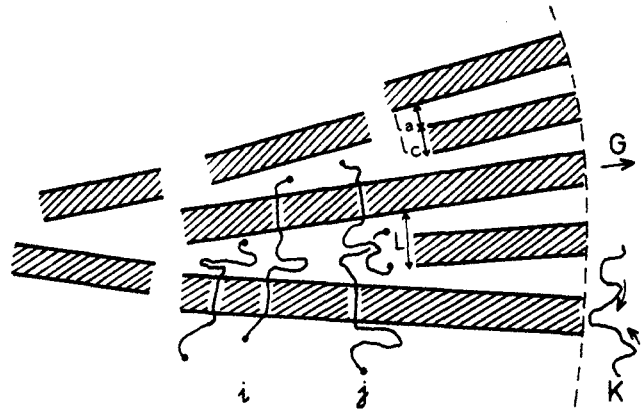

Figure 11. Radial growth of a spherulite. The repulsion between two crystalline lamellae is due to two effects: the trapping of entanglement in the amorphous phase and the nonequilibrium state of the tie chains (see Figure 12).

When two crystallizing lamellae are separated by a distance L of the order (or less) of the mean dimension of the coils, the chains (i) crystallizing and passing through lamellae cannot disentangle. Only chains which end in the amorphous layers can disentangle. In that case $L \leq r_w$, most entanglements are trapped in the amorphous phase. During crystallization the entanglements present in the melted phase are rejected from the place where crystalline layers are formed and restricted to the amorphous layer. Therefore, the density of entanglements in the amorphous phase increases. If n_e is the concentration of entanglements in the equilibrium melted phase, then the increase Δn_e in the concentration of entanglements in the amorphous phase after crystallization of two lamellae separated by a distance L is

$$\Delta n_e = n_e \frac{l_c}{l_a} \delta\left(\frac{r}{L}\right) \qquad L < r \tag{27a}$$

where δ is a function of r/L that depends on the ability of the chain to disentangle during crystallization (the chains are assumed to be monodispersed, $r = r_w$). Obviously, when two lamellae are separated by a distance $L \gg r$, chains (j) in the amorphous phase eliminate their extra entanglements and $\delta = 0$. For the case $L \simeq r$, all the entanglements are trapped and we have $\delta = 1$. As the exact form of the function δ is not important for this discussed, we take the simplest form

$$\delta(r/L) = r/L$$

Then the increase in the number of entanglement in the amorphous layers after crystallization can be written

$$\Delta n_e = n_e \frac{l_c r}{L(L - l_c)} \tag{27b}$$

Obviously the trapping of such entanglements would impede the development of the crystallization for kinetic and thermodynamic reasons.

Kinetic. In the amorphous layer the nucleation and the growth of new crystalline lamellae would be slowed down or even stopped. The effects of cross-links and entanglements on the growth rate is well-known.

Thermodynamic. As the concentration of entanglements in the amorphous phase between crystalline lamellae

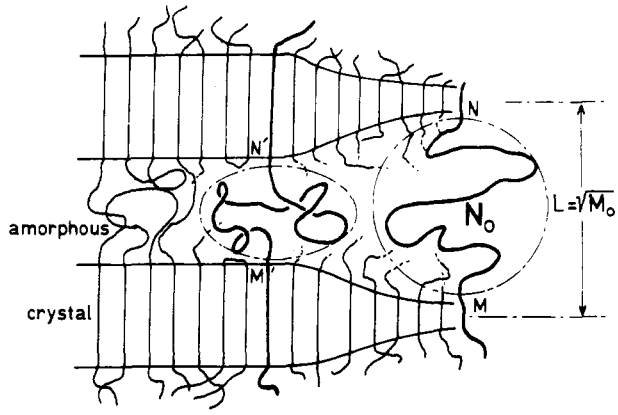

Figure 12. Entropic repulsion between crystalline lamellae in a semicrystalline polymer. A Gaussian chain (MN) at the beginning of crystallization becomes squeezed ($M'N'$) at the end of crystallization if $t_g < t_t$.

is not the same as that in the equilibrium melted phase, one postulates that to each entanglement that has migrated from the crystalline to the amorphous layer must be associated a free energy ΔF_e. This energy can have two origins: (a) each additional entanglement can be visualized as a junction point where the density is locally greater than the equilibrium density of the melted phase; (b) each entanglement reduces the entropy of the chain.

The free energy per unit volume is then

$$\Delta F = +n_e \frac{rl_c}{L(L-l_c)} \Delta F_e - \frac{1}{L} \frac{\Delta H \Delta T}{T_m^0} l_c \qquad (28)$$

Minization gives (for $L > l_c$)

$$L \sim n_e \frac{\Delta F_e}{\Delta H} \frac{T^0_m}{\Delta T} r \sim \frac{r}{\Delta T} \qquad (29)$$

This process could explain the observed correlation law $L \sim r$ and the well-known variations of L with the supercooling ΔT. Obviously this analysis is only valid for $n_e \neq 0$, that is to say for entangled polymers of molecular weight $M > M_e$.

Finally the first term in eq 28 indicates that when two lamellae crystallize, there is a repulsive force $\partial \Delta F/\partial L$ for $r/L < 1$; this is in agreement with the radiating form of spherulite and with the interlamellar crystallization process reported (Figure 11) by Strobl et al.[26b] and others.[64,65]

However, this phenomenological description rests on the assumption that entanglements are well-defined entities and this very likely not true.[61,62] Moreover from this description one cannot predict the order of crystallinity for high molecular weight. In the following section we show that the increase in the free energy (first term in eq 28) during crystallization can come from the deformation of the amorphous chains.

(b) Deformation of the Amorphous Chains during Crystallization. It is well-known that during the crystallization of an extented network the applied stress relaxes; in this process the extended amorphous chains come back to their unperturbed configuration.[75,76] Conversely we think that during the crystallization (in regime II) of an isotropic polymer the amorphous chains are squeezed. This process is illustrated in Figure 12 and is somewhat different from that given by other authors.[77-80] These authors have assumed that the tie points of the crystallizing chains are not located on the same growth front; consequently the amorphous chains between the crystalline lamellae are defomred in an oblate shape (extended conformation). All these theories assume that the ends of the chains are fixed by multinucleation onto the same crystalline lamella and therefore do not predict the observed scaling laws.

Let us focus our attention on an amorphous chain which crystallizes at two different places M' and N' of the growth front of the spherulite, L being the local long period and the mean distance between the two nuclei along the chain. After crystallization of the two stems, the new tie points M'' and N'' of the amorphous chains on the two distinct lamellae are now separated by a distance $r = L - l_c$. This portion of the chain has $N - n_c = L^2/Ca^2 - l_c/a$ monomers (C is the rigidity, n_c the number of monomers per stem) and its equilibrium dimension is $r_0 = [C(N - n_c)a^2]^{1/2} = (L^2 - Cl_ca)^{1/2}$. As r_0 approaches r, the amorphous chain is compressed between the two crystalline lamellae as shown in Figure 12. The entropy of confinement of such a coil is

$$\Delta S = \left(\frac{r_0^2}{r^2} + \frac{r^2}{r_0^2} \right) \simeq \frac{r_0^2}{r^2} \qquad (30)$$

and the free energy per unit volume of the system is

$$\Delta F = -\frac{l_c}{L} \Delta F_c + \frac{KT}{La^2} \frac{L^2 - Cl_ca}{(L - l_c)^2} \qquad (31)$$

ΔF_c being the enthalpy of crystallization per volume, a^3. For simplification one assumes that the monomer has a cubic shape $a = b = c \simeq 1$ Å.

The linear crystallinity being $\chi = l_c/L$ and noting that $L^2 \gg l_ca$, the above relation becomes

$$\frac{\Delta F a^3}{KT} = -\chi\Phi + \frac{a}{l_c} \frac{\chi}{(1-\chi)^2} \qquad (32)$$

The dimensionless parameter $\Phi = \Delta F_c a^3/KT = \Delta H \Delta T/KTT_m^0)a^3$ for a supercooling $\Delta T \simeq 20$ °C is of the order of 0.1.[49,52]

Derivation of the above equation with respect to χ gives (with $l_c \simeq 100$ Å, $a \sim 1$ Å)

$$\ldots + \frac{2\chi}{(1-\chi)^3} + \frac{1}{(1-\chi)^2} = \Phi \frac{I_c}{a} \sim 10 \qquad (33)$$

whose solution is $\chi \simeq 0.5$. Thus the long period L is about twice the value of the crystalline core thickness.

Obviously, the derivation of eq. 33 involves numerous assumptions:

(a) The crystalline lamellae that nucleate at a distance $L \ll M^{1/2}$ have the same growth rate.

(b) The chains crystallize at several places located in the growth front and at a separation of the order of L, the long spacing. When the distance between tie points is greater than L (and/or not located on a same growth front), the chains are not squeezed but stretched: this case has been analyzed by several authors.[77-80] It must be remarked that these authors have minimized the free energy per chain with respect to l_c. In our analysis the situation is rather different; the crystalline core thickness l_c is constant (as noted in section 6.2) and the free energy (eq 31 or 32) is minimized with respect to L (or χ). In both cases, during crystallization the free energy term due to the entropy lost by the confinement of the chains increases and this limits the crystallinity. The assumption of squeezed amorphous chains is in agreement with the neutron scattering experiments of Guenet and Picot.[81]

(c) The Gaussian statistic applies and the first term in eq 30 is assumed negligible ($r_0 \gg r$). It must be recalled here that some type of confinement according to de Gennes does not cost entropy.[82]

(d) The density difference between the two layers cannot be explained if one assumes that every chain crystallizes according the described process. As has been recognized, the drawback of the switchboard model is that it leads to a very high density in the amorphous phase.[83-85] Obviously, all the chains are not squeezed as sketched in Figure 11; dangling chains and chains that have segregated during crystallization can have their unperturbed conformation, and folded chains and extended amorphous chains can also occur. The presence of two types (at least) of amorphous chains in semicrystalline PE has been confirmed by NMR[88,89] and by Raman scattering.[90] Thus the entropy term in eq 31 must be multiplied by a coefficient equal to the proportion of tie molecules in a squeezed conformation. It can be seen, however, that a proportion of one-third of tie molecules, the expected value given by several authors,[85] does not change tremendously the value of χ deduced from eq 33. In the above models we have implicitly postulated that the density difference $\Delta\rho = \rho_c - \rho_a$ between the crystalline and amorphous phases is reduced by other processes such as the diffusion of some chains and the presence of folds. Polymers with very different values of $\Delta\rho$ [positive in general but negative for poly(4-methylpentene-1); see, for example, ref 50] have the same lamellar arrangment; therefore, we think that the difference in density is not the main parameter that controls the morphology of the semicrystalline state. In our view, the phenomenon of chain folding does not play an essential role in the explanation of the lamellar arrangement of semicrystalline polymers obtained by rapid cooling.

Despite these assumptions, eq 33 gives a good estimate of the limiting crystallinity (and of L) obtained for high molecular weight PE. The fact that the amorphous phase is structurally different from the bulk melted phase has been recognized by Manfield[86] and Guenet et al.[81] We emphasize, however, that this crude model cannot explain the dependence of the long period on the molecular weight. A complete theory should take into account both the effects of chain deformation (eq 30) and the variation of the concentration of entanglements in the amorphous phase (eq 27).

7. Conclusion

For semicrystalline polymers crystallized from the melted state by quenching or from the glassy state by annealing above T_g, the weight-average dimension of the coils ($r_w = \sum\omega_i M_i^{1/2}$) is the main parameter that controls the long period, the fluctuation of the long period, the amorphous layer thickness, and the crystallinity. Only the crystalline core thickness is independent of the molecular weight distribution. We summarize the major experimental findings:

(a) The long periods L, L_{cor}, and L_p given by the Bragg, correlation function, and paracrystalline analysis are, for all the polymers studied, linear functions of r_w (eq 2, 8, 12). These functions extrapolate to a value approximately equal to the value of the crystalline core thickness l_c for molecular weight of the order of M_c, the critical mass between entanglements. The master curves $L(M_r)$ and $L_{cor}(M_r)$ can be used to measure with high accuracy the molecular weight M_r of polymers. The difference in L values between polymers of different nature but the same molecular weight comes from the difference in rigidity of the chains, as is expected from the correlation law $L \sim r_w$.

(b) The disorder in the lamellar arrangment measured by the relative width $\Delta\theta/\theta$ of the SAXS peak is proportional to $L - L_{cor}$ (eq 8b) and to $L - L_P$ (eq 11b). It is a linear function of the molecular weight M_r for PE and PTHF and constant for PP and PET; this difference between these two series of polymers is not yet understood.

(c) The interface between crystalline and amorphous layers is sharp and independent of the molecular weight distribution. This conclusion does not rule out the fact that a transition zone having a density gradient can exist in the amorphous layer.

(d) The crystallinity is a linear function of $1/r_w$ and its extrapolates to 1 for a molecular weight of the order of the critical mass between entanglements.

(e) The crystalline core thickness deduced from the measurement of L_{cor} and χ or from the width of the WAXS peak (PET) is independent of the molecular weight distribution. The amorphous layer thickness $l_a = L_{cor} - l_c$ is then a linear function of $r_w = M_r^{1/2}$. From the assertions made in a, d, and e, we conclude that the presence of the amorphous phase in a semicrystalline polymer is due to the presence of entanglements in the melted phase prior to crystallization.

The origin of the correlation law $L \sim l_a \sim r_w = M_r^{1/2}$ is explained by the following arguments.

During crystallization, crystalline lamellae of constant thickness $l_c \sim M^0$, separated by a distance greater than the mean dimension r_w of the coils, nucleate and grow without interaction. When this distance is approximately equal to r_w (or less), the two crystalline lamellae are in interaction via the connecting amorphous chains. During the process of crystallization the amorphous chain is submitted to a tension that propagates along the chain in a time t_t. If this time is greater than the mean growth time $t_G = r/G$, the amorphous chains cannot relax during the crystallization process and the entanglements and amorphous chains are not in an equilibrium state. It has been shown that the relation $t_t = t_G$ defines the critical supercooling rate that separates the two regimes of crystallization. In quenched polymers with $t_t > t_G$, the crystallization is therefore limited by the distortion of the amorphous phase. In the free energy of the crystallizing system, we have taken into account the energy of deformation (entropy term) of the amorphous chain (eq 32) and an energy term proportional to the excess of entanglements (eq 28) occurring in the amorphous phase. The balance between the enthalpy of crystallization and the energy of deformation of the amorphous layers explains the correlation law $L \sim l_a \sim r$, the variation of L with supercooling, and the order of magnitude of the crystallinity for high molecular weight materials (PE).

The relationship between the morphological parameters of the semicrystalline structure (L, l_a, $\Delta L/L$, $\Delta\theta/\theta$) and the weight-average dimension of the coils in the melted state before crystallization is explained neither by the kinetic theories of crystallization nor by the model of crystallization, which assumes short-range order in the melted state.[91,92]

List of Symbols

a	monomer length
C	rigidity, characteristic ratio of a polymer chain
F	fold configuration along a polymer chain in the liquid state
G	growth rate of the crystalline lamellae
$I(s)$	SAXS intensity scattered in direction s
$K(z)$	nonnormalized correlation function
l_c	crystalline layer thickness deduced from the Bragg analysis
l_{cor}	crystalline layer thickness deduced from the correlation function
l_a	amorphous layer thickness
L	long period deduced from the Bragg peak
L_{cor}	long period deduced from the correlation function
L_p	long period deduced from the paracrystalline analysis

L^0, l^0	ordinates at the origin of the various curves $L(M^{1/2})$ and $l_c(M^{1/2})$
$\bar{L}$, $\bar{l}_c$, $\bar{l}_a$	mean values of thicknesses L, l_c, l_a: most probable values of the Gaussian distribution functions $P(L)$, $P(l_c)$, $P(l_a)$
M_c	molecular weight between entanglements
M_i	molecular weight of a chain having N_i monomers
M_n	number-average molecular weight
M_r	r-average molecular weight
M_w	weight-average molecular weight
N	number of links per chain or per portion of chain located in the amorphous phase
n_c	number of atoms per stem in the crystalline state
n_e	concentration of entanglements in the equilibrium melt
$P(l)$	distribution function of the thickness l
Q	SAXS intensity invariant
r_0	end-to-end distance of a chain in the unperturbed state
r	end-to-end distance of a chain in a perturbed state
r_w	weight average of the end-to-end distance of the coils in a polydispersed polymer
s	scattering vector
T_m^0	melting temperature of an infinitely thick crystal
T_c	crystallization temperature
t_t	time necessary for a tension due to crystallization to propagate along the chain
t_g	time for a crystalline lamella to advance over a distance r_0
α	slopes of the curves $L(M^{1/2})$, $L_{cor}(M^{1/2})$, and $L_p(M^{1/2})$
β	slope of the curve $l_c x(M^{1/2})$
γ	slope of the curve $l_a(M^{1/2})$
$\gamma(z)$	normalized correlation function: Fourier transform of $I(s)$
ϵ	slope of the curve $\Delta\theta/\theta(M^{1/2})$
θ	scattering angle
ρ_c, ρ_a	electronic density of the crystalline and amorphous layers
ω_i	mass concentration of chain of mass M_i
χ	crystallinity
Δl_i	fluctuation of the thickness l_i of a layer of type i
ΔF	free energy gained by crystallization
ΔF_c	enthalpy of crystallization per unit volume
Δn_e	difference in the concentration of entanglements between the melted and the amorphous phase of the semicrystalline state
ΔT	supercooling $T_m^0 - T_c$
$\Delta\rho$	density difference between crystalline and amorphous phases
$\Delta\theta/\theta$	relative width of the SAXS intensity peak

Registry No. PE, 9002-88-4; PET, 25038-59-9; PTHF, 24979-97-3; PTHF (SRU), 25190-06-1; PP, 9003-07-0.

References and Notes

(1) Mandelkern, L. *Crystallization of Polymers*; McGraw-Hill: New York, 1964.
(2) Mandelkern, L. *Faraday Discuss. Chem. Soc.* **1979**, *68*, 310.
(3) Maxfield, J.; Mandelkern, L. *Macromolecules* **1977**, *10*, 550.
(4) Glotin, M.; Mandelkern, L. *Colloid Polym. Sci.* **1982**, *260*, 182.
(5) Hoffman, J. D.; Frolen, L. J.; Ross, G. S.; Lauritzen, J. I. *J. Res. Natl. Bur. Stand., Sect. A* **1975**, *A59*, 677.
(6) Ergoz, E.; Fatou, J. G.; Mandelkern, L. *Macromolecules* **1972**, *5*, 147.
(7) Robelin-Souffaché, E.; Rault, J. *J. Phy. (Les Ulis, Fr.)* **1980**, *41*, 1459; *J. Phys. (Les Ulis, Fr.)* **1980**, *41*, 1469. Rault, J.; Robelin-Souffaché, E. *J. Phys. (Les Ulis, Fr.)* **1982**, *43*, 1437.
(8) ben Cheick Larbi, F.; Hert, M.; Grenier, M. F.; Rault, J. *Macromolecules* **1985**, *164*, 18.
(9) Rault, J.; Robelin-Souffaché, E.; Perez, G. *J. Macromol. Sci., Phys.* **1983**, *B22*, 575.
(10) Hsiue, E. S.; Robertson, R. E.; Yeh, G. S. *J. Macromol. Sci., Phys.* **1983**, *B22*, 305.
(11) Zachmann, H. G.; Wiswe, D.; Gehrke, R.; Riekel, C. *Macromol. Chem. Phys., Suppl.* **1985**, *No. 12*, 175.
(12) Rault, J. *CRC Crit. Rev. Solid State Mater. Sci.* **1986**, *13*, 57.
(13) Voight-Martin, I. G.; Mandelkern, L. *J. Polym. Sci., Polym. Phys. Ed.* **1982**, *19*, 1769.
(14) Voight-Martin, I. G.; *Macromolecules* **1984**, *17*, 321.
(15) Voigt-Martin, I. G.; Mandelkern, L. *J. Polym. Sci., Polym. Phys. Ed.* **1984**, *22*, 1901.
(16) Voigt-Martin, I. G.; Fischer, E. W.; Mandelkern, L. *J. Polym. Sci., Polym. Phys. Ed.* **1980**, *18*, 2347.
(17) (a) Flory, P. J. *Principles of Polymer Chemistry*; Cornell University Press: Ithaca, NY, 1953. (b) Flory, P. J. *Statistical Mechanics of Chain Molecules*; Interscience: New York, 1969.
(18) Vonk, C. G.; Kortleve, G. *Kolloid Z. Z. Polym.* **1967**, *220*, 19.
(19) Kortleve, G.; Vonk, C. G. *Kolloid Z. Z. Polym.* **1968**, *225*, 124.
(20) Hosemann, R.; Bagghi, S. N. *Direct Analysis of Diffraction by Matter*; North-Holland: Amsterdam, 1962.
(21) Debye, P.; Anderson, H. R.; Brumberger, H. *J. Appl. Phys.* **1957**, *28*, 679.
(22) Porod, G. *Kolloid Z. Z. Polym.* **1951**, *124*, 83.
(23) Porod, G. In *Small Angle X-Ray Scattering*; Glatter, O., Kartky, O., Eds.; Academic Press: New York, 1982.
(24) Ruland, W. J. *J. Appl. Cryst.* **1971**, *4*, 70.
(25) Strobl, G. R.; Schneider, M. *J. Polym. Sci., Polym. Phys. Ed.* **1980**, *18*, 1347.
(26) Strobl, G. R.; Schneider, M.; Voigt-Martin, I. E. *J. Polym. Sci., Polym. Phys. Ed.* **1980**, *18*, 1361.
(27) Tsvankin, D. *Vysokomol. Soedin.* **1964**, *6*, 2304.
(28) Buchanam, D. R. *J. Polym. Sci., Polym. Phys. Ed.* **1971**, *9*, 645.
(29) Slutsker, L. I. *Vysokomol. Soyed.* **1975**, *A17*, 262.
(30) (a) Reckinger, C.; Rault, J. *J. Phys. (Les Ulis, Fr.)* **1986**, *47*, 163. (b) Reckinger, C. Thesis, Orsay, 1985.
(31) Reckinger, C.; ben Cheick Larbi, F.; Rault, J. *J. Macromol. Sci., Phys.* **1984**, *B23*, 511.
(32) Souffaché, E.; Perez, G.; Lecluze, C.; Rault, J., to be published in *J. Macromol. Sci., Phys.*
(33) Gorin, S. *J. Chem. Phys.* **1968**, *65*, 2069; **1968**, *65*, 2084.
(34) Geny, F. Thesis, Paris, 1977.
(35) Schultz, J. M. *Bull. Am. Phys. Soc.* **1980**, *25*, 249.
(36) Rault, J.; Robelin-Souffaché, E., to be published in *J. Polym. Sci., Phys.*; paper 2 in this series.
(37) Richards, R. B. *J. Appl. Chem.* **1951**, *1*, 370.
(38) Burch, G.; Field, G.; McTigue, F.; Spurlin, H. *SPE J.* **1957**, *13*, 34.
(39) Wakelin, J. H,; Virgin, H. S.; Crystal, E. *J. Appl. Phys.* **1959**, *30*, 1654.
(40) Alexander, L. E. *X-Ray Diffraction Methods in Polymer Science*; Wiley: New York, 1969.
(41) Statton, W. O. *J. Appl. Polym. Sci.* **1963**, *7*, 803.
(42) Sotton, M.; Arniaud, A. M.; Rabourdin, C. *J. Appl. Polym. Sci.* **1978**, *22*, 2585.
(43) Ferry, J. D. *Viscoelastic Properties of Polymers*; Wiley: New York, 1970.
(44) Lieser, G.; Fischer, E. W.; Ibel, K. *J. Polym. Ed. Polym. Lett. Ed.* **1975**, *13*, 39.
(45) Capaccio, C.; Ward, I. M.; Wilding, M. A.; Longman, G. W. *J. Macrom Sci., Phys.* **1978**, *B15*, 381.
(46) (a) Schelten, J.; Ballard, D. G.; Wignall, G. D.; Longman, G.; Schmatz, W. *Polymer* **1976**, *17*, 751. (b) Ballard, D. E.; Burgess, A. N.; Crowley, T. L.; Longman, G. W. *Faraday Sicuss. Chem. Soc.* **1979**, *68*, 279.
(47) Stamm, M.; Fischer, E. W.; Dettenmaier, M. D. *Faraday Discuss. Chem. Soc.* **1979**, *68*, 263.
(48) Guenet, J. M.; Picot, C.; Benoit, H. *Faraday Discuss. Chem. Soc.* **1979**, *68*, 251.
(49) Yoon, D. Y.; Flory, P. J. *Faraday Discuss. Chem. Soc.* **1979**, *68*, 388.
(50) Geil, P. H. *Polymer Single Crystals*; Wiley: New York, 1963.
(51) Lauritzen, J. I.; Hoffman, J. D. *J. Res. Natl. Bur. Stand. (U.S.)* **1960**, *64A*, 73; *J. Appl. Phys.* **1973**, *44*, 4340.
(52) Hoffman, J. D.; Guttman, C. M.; Dimarzio, E. A. *Faraday Discuss. Chem. Soc.* **1979**, *68*, 177.
(53) Rault, J. *J. Phys. Lett. (Les. Ulis, Fr.)* **1978**, *39*, L411; *Faraday Discuss. Chem. Soc.* **1978**, *68*, 403.
(54) Rault, J. *C. R. Acad. Sci. Ser. II* **1977**, *285B*, 321.
(55) Rault, J. *J. Macromol. Sci., Phys.* **1978**, *B15*, 567.
(56) Rault, J. In *Plastic Deformation of Amorphous and Semi-Crystalline Material*; Edition de Physique; Escaig, G'sell, Eds.; 1982, p 313.
(57) Point, J. J. *Faraday Discuss. Chem. Soc.* **1979**, *68*, 167; *Macromolecules* **1979**, *12*, 770.
(58) Allegra, G. *J. Chem. Phys.* **1977**, *66*, 5453.
(59) Cuttler, D. J.; Hendra, P. J.; Sang, R. D. *Faraday Disc. Chem. Soc.* **1979**, *68*, 320.
(60) Rault, J. *Faraday Discuss. Chem. Soc.* **1979**, *68*, 370.
(61) Graessley, . W.; Edwards, S. F. *Polymer* **1981**, *22*, 1329.
(62) Rault, J. *Non-Newtonian Fluid Mech.* **1987**, *23*, 229; *C. R. Acad. Sci.* **1985**, *300II*, 433.
(63) Posthuma de Boer, A.; Pennings, A. J. *Faraday Discuss. Chem. Soc.* **1969**, *68*, 345.

(64) Lemstra, P. J.; Schouten, A. J.; Challa, G. J. *J. Polym. Sci., Polym. Phys. Ed.* **1974**, *12*, 1565.
(65) Warner, F. P.; Brown, D. S.; Wetton, R. E. *Polymer* **1981**, *22*, 1349.
(66) Keith, H. D.; Padden, J. F. *J. Polym. Sci.* **1959**, *41*, 525; *J. Appl. Phys.* **1964**, *35*, 1270.
(67) Yeh, G.; Lambert, S. L. *J. Polym. Sci., Polym. Phys. Ed.* **1972**, *10*, 1183.
(68) Warner, F. P.; Macknight, W. J.; Stein, R. S. *J. Polym. Sci., Polym. Phys. Ed.* **1977**, *15*, 2113.
(69) Gedde, U. W.; Janson, J. F. *Polymer* **1985**, *26*, 1469.
(70) Wunderlich, B. *Faraday Discuss. Chem. Soc.* **1979**, *68*, 239.
(71) de Gennes, P.-G. *Faraday Discuss. Chem. Soc.* **1979**, *68*, 381.
(72) Dimarzio, E. A.; Guttman, C. M.; Hoffman, J. D. *Faraday Discuss. Chem. Soc.* **1979**, *68*, 210.
(73) Törmälä, P. *J. Macromol. Sci., Rev. Macromol. Chem.* **1979**, *C17*, 297.
(74) Patterson, G. D. CRC *Crit. Rev. Solid State Mater. Sci.* **1980**, *9*, 373.
(75) Flory, P. J. *J. Chem. Phys.* **1947**, *15*, 397.
(76) Flory, P. J. *J. Chem. Phys.* **1949**, *17*, 224.
(77) Tung, L. H.; Buckser, S. *J. Phys. Chem.* **1958**, *62*, 1530.
(78) Roe, R. J.; Smith, K. J.; Krigbaum, W. *J. Chem. Phys.* **1961**, *35*, 1306.
(79) Krigbaum, W. R.; Uematsu, I. *J. Polym. Sci., Part A* **1965**, *3*, 2915.
(80) Elyashevitch, G. K.; Baranov, V. G.; Frenkel, S. Y. *J. Macromol. Sci., Phys.* **1977**, *B13*, 255.
(81) Guenet, J. M.; Picot, C. *Macromolecules* **1981**, *14*, 309.
(82) de Gennes, P.-G. *C. R. Acad. Sci. Series II* **1979**, *B289*, 103; **1980**, *B290*, 519.
(83) Frank, F. C. *Faraday Discuss. Chem. Soc.* **1979**, *68*, 7.
(84) Guttman, C. M.; di Marzio, E. A. *Macromolecules* **1982**, *15*, 525.
(85) Manfield, M. L.; Guttman, C. M.; di Marzio, E. A. *J. Polym. Sci., Part C: Polym. Lett.* **1986**, *24*, 565.
(86) Manfield, M. L. *Macromolecules* **1987**, *20*, 1384.
(87) Fischer, E. W. *Pure Appl. Chem.* **1978**, *50*, 1319.
(88) Fischer, E. W.; Schmidt, G. *Angew. Chem.* **1962**, *551*, 74.
(89) McBrierty, V. J. *Faraday Discuss. Chem. Soc.* **1979**, *68*, 78.
(90) Strobl, G. L.; Hagedorn, W. J. *J. Polym. Sci., Polym. Phys. Ed.* **1978**, *16*, 1329.
(91) Yeh, G. S. *J. Macromol. Sci. Phys.* **1972**, *B6*, 451.
(92) Pechhold, W. R. *Colloid Polym. Sci.* **1980**, *258*, 269.

Morphology and Chemical Properties of the Dow Perfluorosulfonate Ionomers

Robert B. Moore, III,† and Charles R. Martin*

Department of Chemistry, Texas A&M University, College Station, Texas 77843.
Received October 19, 1988; Revised Manuscript Received February 10, 1989

ABSTRACT: The Dow Chemical Co. has developed an interesting new class of perfluorosulfonate ionomers (PFSI's). We have conducted a broad-based investigation of the supermolecular structures of these PFSI's. Small-angle X-ray scattering data showed that the Dow PFSI's contain ionic clusters. The sizes of these clusters vary with equivalent weight and water content. Wide-angle X-ray diffraction and differential scanning calorimetry demonstrated that PFSI's with equivalent weights greater than ca. 800 g/mol are partially crystalline. The extent of crystallinity increases with equivalent weight. Surprisingly, the melting point of the Dow PFSI's varied only slightly with equivalent weight. This suggests that these are block-type copolymers. We have also developed dissolution and solution-casting procedures for a wide range of equivalent weights of these PFSI's.

Introduction

Perfluorosulfonate ionomers (PFSI's) are cation-conducting polymers with good chemical and thermal stabilities.[1-4] These polymers have been used in a variety of electrochemical processes and devices including chloralkali cells,[3,4] fuel cells,[5] water electrolyzers,[6] and polymer-modified electrodes.[7-12] The Nafion polymers (Du Pont, structure I) have been the most extensively studied PFSI's.

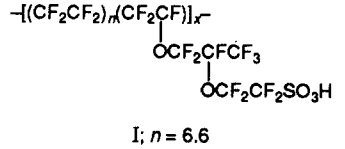

I; $n = 6.6$

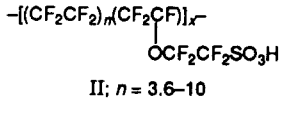

II; $n = 3.6$–10

Recently, the Dow Chemical Co. has developed a new class of PFSI's. The Dow PFSI's (structure II) contain a shorter side chain than the Nafion polymers. We have obtained samples of various equivalent weights of the Dow polymers, and we are evaluating the performances of these polymers in fuel-cell applications.[13,14] In support of this work, we have conducted fundamental investigations of the solubilities and the chemical and morphological properties of the Dow PFSI's. We report the results of these and related investigations here.

† Current address: Department of Chemistry, McGill University, 801 Sherbrooke Street West, Montreal, Quebec, Canada H3A 2K6.

Table I
Dissolution Conditions for the Na^+-Form Dow PFSI's

equiv wt	time, h	temp, °C	solvent
635	1	250	ethanol–water
803	3	250	ethanol–water
909	3	250	ethanol–water
1076	3	275	ethanol–water
1269	3	300	1-propanol–water

Experimental Section

Materials. H^+-form PFSI membranes, having equivalent weights of 635, 803, 909, 1076, and 1269 g/mol of $-SO_3^-$ sites, were obtained from the Dow Chemical Co. The as-received membranes were refluxed in 8 M HNO_3 (for ca. 24 h) to remove discoloring impurities. The membranes were then converted to the Na^+ form by soaking overnight in 1 M NaOH. Excess NaOH was removed by thoroughly rinsing the membranes with purified water. Ag^+-form PFSI was prepared by soaking the membranes in 1 M $AgNO_3$ for 24 h. Quenched Na^+-form PFSI samples were prepared by heating the membranes, in a muffle furnace (350 °C), and then rapidly cooling in liquid N_2.

Instrumental Methods. The wide-angle X-ray diffraction (WAXD) studies were conducted on dry, Na^+-form membranes.[15] Differential scanning calorimetry (DSC) data were obtained as described previously.[15] Small-angle X-ray scattering (SAXS) experiments were performed using the Oak Ridge National Laboratory 10-m SAXS system with a 2-dimensional position-sensitive proportional counter. The rotating anode X-ray source was operated at 40 kV and 60 mA. SAXS analyses were performed on hydrated, Na^+-form and dry, Ag^+-form PFSI membranes. The Na^+-form PFSI samples were hydrated by boiling in water for

0024-9297/89/2222-3594$01.50/0